Magnetoelectric Flexural Gate Transistor with NanoTesla Sensitivity

Feng Li, Rajiv Misra, Zhao Fang, Yufei Wu, Peter Schiffer, Qiming Zhang *IEEE Fellow*, Srinivas Tadigadapa *Senior Member*, *IEEE*, and Suman Datta *Senior Member*, *IEEE*

***Abstract*— Magnetic sensors capable of detecting tiny ac magnetic fields ranging from micro-Tesla to picoTesla are of great interest. In this paper, we demonstrate an integrated magnetoelectric flexural gate transistor (MEFGT) with nanoTesla magnetic field detection sensitivity at room temperature. The device capacitively couples a Metglas® ($Fe_{0.85}B_{0.05}Si_{0.1}$) based magnetostrictive unimorph micromechanical cantilever beam to the gate of an n-channel field effect transistor. Using this sensor configuration, a sensitivity of 0.23 mV/μT and a minimum detectable field of 60 nT/√Hz at 1 Hz and 1.5 mV/μT and 150 pT/√Hz at the flexural resonance of the cantilever structure of 4.9 kHz were obtained. The results demonstrate a significant improvement in the thin film ME sensor integration with standard CMOS process and open the possibility of monolithic magnetic sensor arrays fabrication for biomedical imaging applications.**

***Index Terms*— Magnetoelectric (ME), magnetostriction, Metglas® ($Fe_{0.85}B_{0.05}Si_{0.1}$) thin films, microelectromechanical systems (MEMS), magnetoelectric flexural gate transistor (MEFGT).**

I. Introduction

ACCURATE measurements of tiny magnetic fields are of great interest in different applications. Medium accuracy sensors such as anisotropic magnetoresistive (AMR) and giant magnetoresistive (GMR) sensors have a resolution around 10 nT. While fluxgate sensors have been demonstrated to measure DC and low frequency ac fields up to 1 mT with a resolution of 10 pT, they typically have a large footprint with centimeter sized coil and are not amenable to miniaturization into array format [1-3]. Till date, measurement of magnetic fields below picoTesla signal can only be performed with the most sensitive magnetic sensors – superconducting quantum interference device (SQUID) [4], which are typically used in high precision scientific experiments and in biomedical imaging applications. In recent years, laboratory studies on magnetoelectric (ME) effect [5-6] sensors have sparked interest in the quest towards achieving low cost, room temperature and ultra-sensitive magnetometers. Such bulk sensors constructed from ME laminates were reported to exhibit large ME coupling coefficient of 21.46 V/cm•Oe [7] and a resolution of 2×10^{-11} T/√Hz at resonance [8].

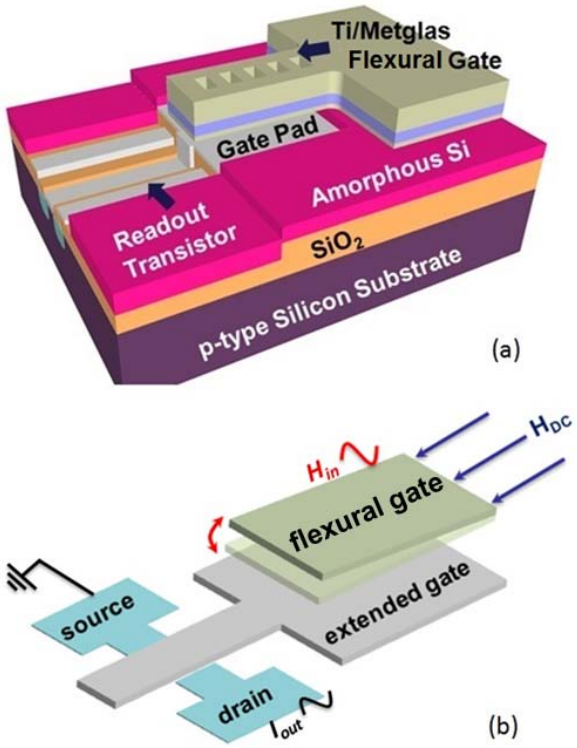

Fig. 1. (a) Schematic of the magnetoelectric flexural gate transistor (MEFGT). (b) The principle of operation of a magnetoelectric flexural gate transistor (ME FGT).

In consideration of the need for high spatial resolution of magnetic field sensing applications, the current challenges in the state of the art pertain to the realization of high sensitivity magnetic sensor arrays. Motivated by this challenge, in this paper, we introduce a new type of chip-scale magnetic sensors – a magnetoelectric flexural gate transistor (MEFGT) sensor by integrating a magnetostrictive (MS) Metglas® ($Fe_{0.85}B_{0.05}Si_{0.1}$) thin film micromechanical cantilever directly atop a sensing and amplifying transistor, as shown in Figure 1(a). The device combines the merits of magnetoelectric laminates [9] with the concepts of a flexural-gate transistor [10]. The direct integration of the Metglas® films on the MOS circuit provides the advantages of high reliability, small size,

Manuscript received xx, 2012. This research was supported by the National Science Foundation under Grant No. ECCS-0824202. We also appreciate the support from MRSEC DMR-0820404.

F. Li, Z. Fang, Y. Wu, S. Tadigadapa, Q. Zhang, and S. Datta are with Department of Electrical Engineering, The Pennsylvania State University, University Park, PA 16802 USA (e-mail: fxl135@psu.edu).

R. Misra and P. Schiffer are with Department of Physics, The Pennsylvania State University, University Park, PA 16802 USA.

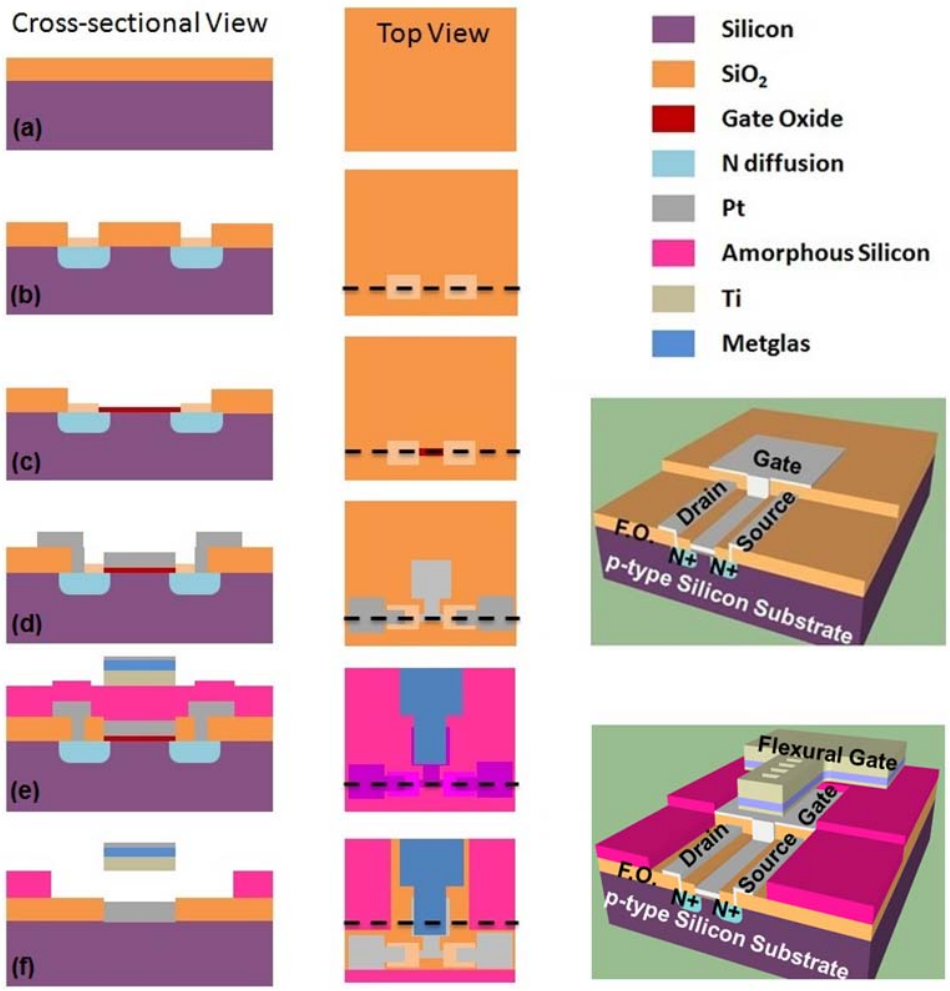

Fig. 2. Schematic of the fabrication process (not to scale). (a) Deposition of 1 μm thermal field oxide on p-type silicon wafer. (b) Pattern and wet etch field oxide for source drain formation via solid source diffusion. (c) Gate oxide pattern and deposition. (d) Gate electrode metallization using liftoff process. (e) Deposition of 500 nm-thick amorphous silicon for the sacrificial layer and lift-off Metglas/Ti. (f) Patterning to prevent unwanted undercutting during release step and release cantilever structure using XeF_2 isotropic etching.

low dielectric loss, and vector sensing capability of magnetic fields [11]-[13].

II. Principle of Operation

The MEFGT device consists of a freestanding unimorph cantilever made of magnetostrictive Metglas® film on a passive titanium film and is located directly atop an extended gate of a MOS readout transistor and with a small air gap in between [9]. Time varying ac magnetic field induces flexural bending motion in the suspended cantilever via magnetostriction effect which, in turn, modulates the air-gap capacitance. The air-gap capacitance modulation is sensed directly via modulation of the channel charge density in the field effect transistors (FETs) and is amplified by the transconductance of the FETs in the form of drain current modulation (Fig 1(b)). Therefore, the MEFGT combines the benefits of high-deflection property of MS cantilever sensors with FET based motion sensing and amplification.

III. Fabrication of MEFGT

The major fabrication process steps shown in Figure 2 include the following: 1) standard NMOS transistor fabrication processes (Figure 2(a) – (d)); 2) deposition of the sacrificial layer; 3) deposition and patterning of mechanically active structure (Figure 2(e)); and 4) final anneal and release (Figure 2(f)). A total of six photolithographic steps were used in the fabrication of the MEFGT.

The fabrication process began with the growth of a 1 μm thick field oxide (SiO_2) [thermal oxidation at 1050°C at for 3 hours] on a single-side-polished, 10^{15} cm^{-3} doped, (100) p-type silicon wafer. This is followed by an NMOS fabrication process that includes formation of n^+ doped source drain structures via liquid source diffusion [20 min $POCl_3$ pre-deposition at 1000°C and 30 min, and 1050°C wet oxidation drive-in], gate oxide growth [950°C 30 min dry oxidation and 30 min post anneal] and gate electrode metallization [10 nm/100 nm thick Ti/Pt metal deposition [via RF sputtering at 200 W power under 5 mTorr pressure]. For the fabrication of the transistors, four photolithography steps were used for source/drain window patterning, gate oxide deposition, contact

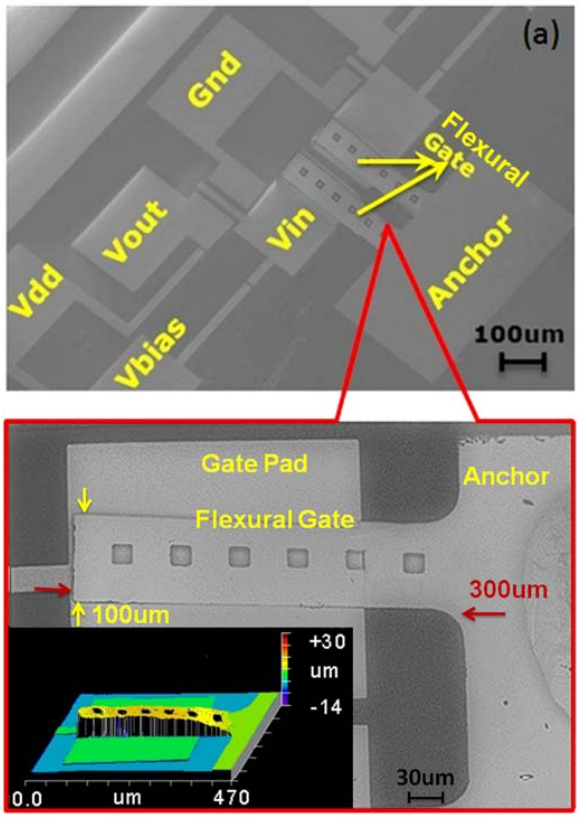

Fig. 3. (a) Scanning Electron Microscopy (SEM) of magnetoelectric flexural gate transistor (MEFGT). (b) Zoomed SEM image of the 300 μm long and 100 μm wide flexural gate atop the gate pad. (Inset: White light optical interference microscope (Zygo® NT100) image of the freestanding magnetostrictive top flexural cantilever gate structure)

via etching, and electrode patterning (Figure 2 (b) - (d)). This is followed by the fabrication of the top flexural gate structure, for which a 500 nm amorphous silicon was chosen as the sacrificial material, deposited by plasma enhanced chemical vapor deposition [PECVD using Ar and SiH_4 precursors, RF power of 200 W at 2 Torr, 220 °C)]. Next, a 500 nm thick layer of titanium was deposited followed by ion beam sputtering of 100 nm thick Metglas® film, and were patterned using a lift-off technique to form a 300 μm × 100 μm MS cantilever, as shown in Figure 2 (e). A DC magnetic field of 600 Oe was applied to polarize the Metglas® film domains during the deposition process [14, 15]. Finally, the cantilever structures were released by a xenon difluoride (XeF_2) vapor phase etching process and annealed at 350°C (to release internal stress) (Figure 2 (f)). The use of an amorphous silicon sacrificial layer ensures a rapid release of the cantilever structure while the use of the XeF_2 vapor phase etching minimizes any damage of the transistor gate oxide and provides high selectivity to photoresist protection mask used to prevent the lateral undercutting of the anchor areas. Figure 3(a) and (b) show the SEM image of MEFGT and the freestanding cantilever gate structure, respectively. The inset of Figure 3 (b) shows that the top flexural gate is bent-up by ~5 μm at the tip end due to a larger residual tensile stress in the Metglas® film in comparison to the Ti passive layer leading to a decrease in the air gap capacitance.

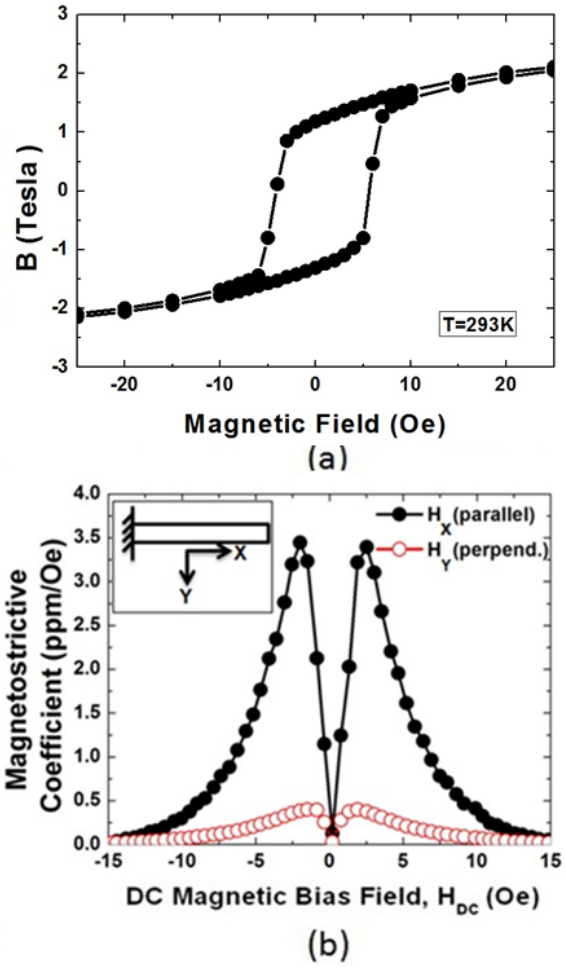

Fig. 4. (a)) B-H hysteresis loop. (b) Magnetostrictive coefficient as a function of the in-plane applied magnetic field.

IV. MEFGT Characterization

A. Film Characterization

The magnetic properties of the deposited Metglas® thin film were characterized in magnetic properties measurement system [Quantum Design Inc. MPMS System] [16]. The films show a low coercivity of ~6 Oe and high magnetization ~2 Tesla, as shown in Figure 4(a). Magnetostrictive coefficient of the films was characterized by using a laser vibrometer setup. The entire sample was placed in a custom made Helmholtz coil and the deflection of the cantilever tip was accurately measured as a function of the applied magnetic field. The applied magnetic field using the Helmholtz coil was accurately calibrated using a LakeShore 450 Gaussmeter. Figure 4 (b) shows the measured magnetostrictive coefficient as a function of the applied in-plane magnetic field. The maximum magnetostrictive coefficient in the perpendicular direction (i.e. applied magnetic field is orthogonal to the magnetization (poling) direction of the Metglas® film) is ~7 times smaller than in the parallel direction and therefore provides a clear directional (vector) sensitivity to the applied magnetic field.

The performance of the top flexural gate capacitor as a function of applied magnetic bias field was measured using an Andeen Hagerling Inc. AH 2700A ultra-precision capacitance

bridge at 100 Hz. The air-gap capacitance as a function of the applied magnetic field is shown in Figure 5. The derivative of this curve defined as the differential capacitance between the top flexural gate and the extended transistor gate pad as a function of the applied magnetic bias field is also shown in Figure 5. As expected, the capacitance changes as a function of the applied magnetic field due to the magnetostrictive effect in Metglas®. The asymmetric differential response can be explained by the slight asymmetry in the coercive fields seen in the B-H loop (Fig. 4(a)) in the sputtered films. The differential capacitance peaks occur at 5 Oe & -7 Oe which are different than the bias magnetic field of 2.5 Oe at which the peak values in magnetostriction coefficient is obtained in Figure 4(b). This is due to the fact that the two different MS cantilevers were used in these measurements and the two cantilever films had undergone different deposition and fabrication steps and have slightly different aspect ratios which can alter the magnetization profiles in the films.

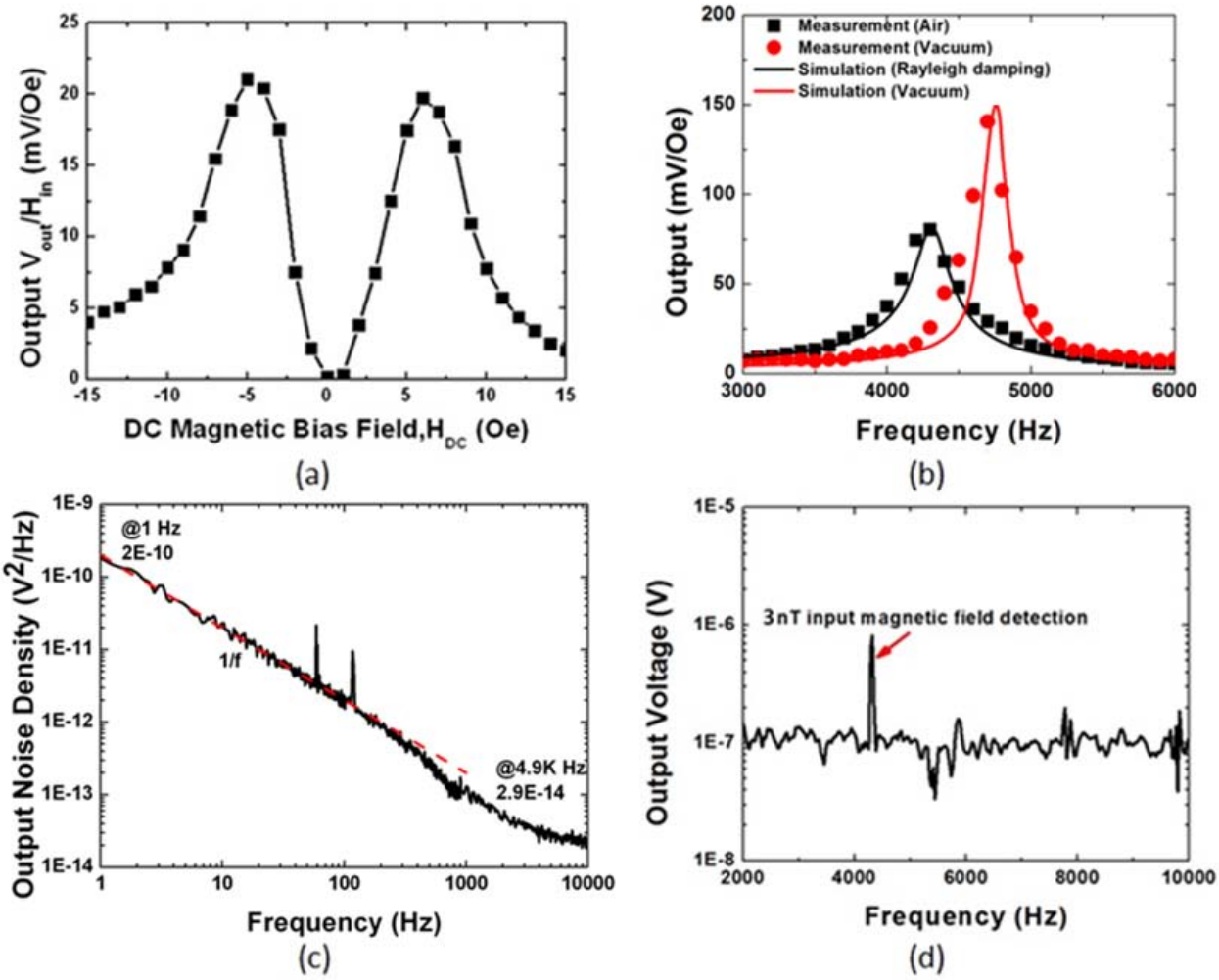

Fig. 7. (a) Low frequency output voltage as a function of the DC magnetic field. The data was measured at 20 Hz and H_{in} = 0.38 Oe. (b) MEFGT frequency response measurement and simulation in both air and vacuum. (c) Output noise performance of MEFGT. (d) Frequency spectrum of 3 nanoTesla input ac magnetic field in air. (The DC magnetic bias field is set at 7 Oe. 3nT ac magnetic field is the minimum generated by the measurement setup.)

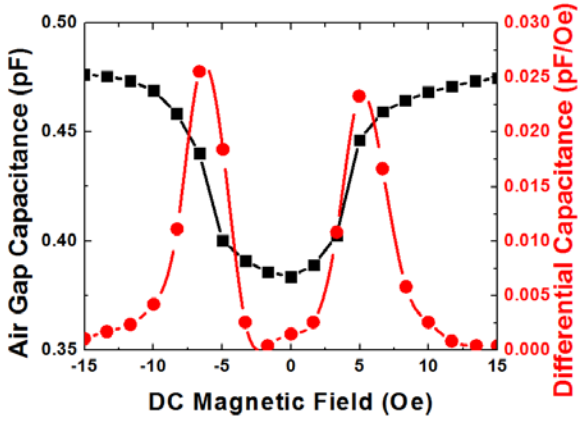

Fig. 5. Flexural gate air gap capacitance (black) and differential capacitance (red) as a function of the applied magnetic bias field.

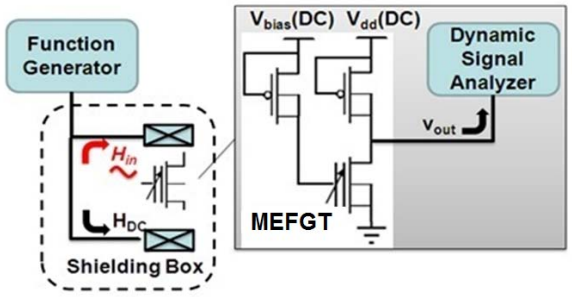

Fig. 6. Schematic of ac magnetic field measurement set-up. H_{in} is the ac magnetic field to be detected. H_{DC} is the DC bias magnetic field. The magnetic field was calibrated using a LakeShore 450 Gaussmeter (Hall probe model HMMT-6J04-VF).

B. *Device Characterization*

The devices were placed in a dual-in-line package and electrical connections were made via conventional wire bonding. The performance of the MEFGT was thereafter characterized using the configuration illustrated in Figure 6. These measurements were performed in a magnetically shielded iron box to prevent unwanted interference from earth's magnetic field and other stray electromagnetic noise. An electromagnet driven by a function generator which included an appropriately set current, provided both input ac magnetic field, H_{in} (signal) and the bias magnetic field, H_{DC} (for maximum sensitivity). The output transistor voltage was measured using a Stanford Research SRS-830 lock-in amplifier and a 35670A HP dynamic signal analyzer (DSA).

Figure 7 (a) shows the low frequency (20 Hz) output voltage of the transistor integrated with the MS cantilever as a function of the applied DC magnetic bias field as measured by the common source readout amplifier circuit for a 0.38 Oe input ac magnetic field. The result shows that the output voltage follows the input capacitance change with DC magnetic bias field.

The resonance response of the MEFGT was studied both in air and vacuum (10^{-3} Torr), as shown in Figure 7(b). The vacuum measurement was performed in a separate setup. A custom-made Helmholtz coil was used to generate the ac input magnetic field while the DC bias field was provided by a permanent magnet placed inside the chamber. The use of the permanent magnet avoids the coil from overheating due to the passage of large dc current. The magnetic field of the magnet was also calibrated by the Gaussmeter and the position of the sensor was adjusted to match the bias field corresponding to maximum output. The entire set-up was pumped down to mTorr pressure range using a dry pump. After the vacuum (pressure) in the chamber stabilized, the chamber was valved off and physically disconnected from the pumping system to isolate it from the undesired mechanical vibration of the pump. The output of the sensor was measured by sweeping the frequency of the magnetic field at constant amplitude. The device resonance frequencies and the *Q*-factor were determined to be 4.27 kHz and 12 (in air) and 4.9 kHz and 24 (in vacuum) respectively. At resonance, the output voltage increases by ~10 times (in air) and ~20 times (in vacuum) in comparison to the off resonance output. The observed resonance behavior in both air and vacuum was confirmed using a modal analysis in COMSOL® finite element multi-physics software [17]. By adjusting the mass damping parameter in the Rayleigh damping model, we were able to match the frequency response in air.

The noise spectrum of MEFGT is shown in Figure 6 (c). The flicker noise of the input transistor limits the noise floor of the entire system. From Figs 7 (a), (b), & (c), we obtain a sensitivity of 0.23 mV/μT @ 1 Hz corresponding to a minimum detectable field of 60 nT/√Hz @ 1 Hz, and a sensitivity of 1.5 mV/μT at the resonance frequency of 4.27 kHz corresponding to a minimum detectable field of 150 pT/√Hz. In Figure 7(d), we demonstrate the detection of 3 nano Tesla input magnetic signal at the resonant frequency. This result represents a significant enhancement in comparison to the first integrated ME sensor demonstrated by Y. Lu and A. Nathan with 40 micro Tesla detectable field [18].

V. Modeling

To better understand the MEFGT performance, we will investigate the two main factors that limit the performance of the device in this following section.

The input charge signal originating from the flexural gate displacement can be expressed as

$$q_{in} = \Delta C * V_{bias} \quad (1)$$

where q_{in} is the input gate charge, ΔC is the differential capacitance and V_{bias} is the potential difference across the flexural gate and transistor gate. Due to the stress mismatch in the constituent layers, the parallel plate assumption for C_0 is no longer valid. In order to better understand the effect of the non-ideal air gap of the fabricated devices, a more accurate formulation of the capacitance is required and is modeled next.

A. *Capacitance Modeling*

The analytical model of the static characteristics of the microcantilever expresses the relation between the applied magnetic field and the differential capacitance. The parallel plate capacitance between the freestanding MS cantilever and the gate electrode was modeled by accounting for the anticlastic bending of the cantilever. A schematic illustration of the cantilever is shown in Figure 8(a). Applying a two-

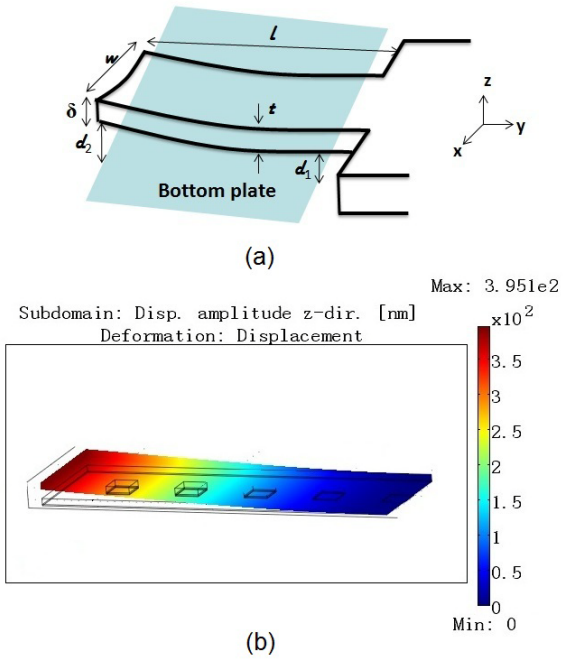

Fig. 8. Three-dimensional view of the cantilever to express (a) analytical 2D Bow approximation and (b) COMSOL 3D simulation structure.

dimensional (2D) bowing approximation, which results from the 2D residual stress, we extract two parameters, effective area, A_{eff} and effective gap, d_{eff}. The effective shape along the width direction using a polynomial curve fitting from the white light interference microscope image can be approximated as

$$w_{eff}(d) = w(1-0.2\frac{(d-0.5)^2}{w}) \quad (2)$$

where w is the cantilever width and d is the distance between cantilever (top flexural gate) and bottom plate (transistor gate pad). Correcting for the fringing field effect, cantilever release via holes, and the cantilever length, the effective area A_{eff} is expressed as

$$A_{eff} = \alpha(A)\int_d w(1-0.2\frac{2(d-0.5)}{w})\Delta d \quad (3)$$

where ε_0 is air permittivity and $\alpha(A)$ is the correction factor. In a similar method from the empirical bending profile of the cantilever, an approximation for the effective gap d_{eff} can be obtained as follows:

TABLE I
PARAMETERS FOR RESONANT GATE

Symbol	Discription	Value
E_P	Young's modulus for Ti, (GPa)	116
E_M	Young's modulus for Metglas, (GPa)	110
t_p	Thickness modulus for Ti, (nm)	500
t_m	Thickness modulus for Metglas, (nm)	100
ρ_p	Density for Ti, (g/cm^3)	4.5
ρ_m	Density for Metglas, (g/cm^3)	7.7
w	Width of resonant gate, (μm)	100
l	Length of resonant gate, (μm)	300
ε_0	Permittivity of air, (F/m)	8.84e-12
$d_{31}{}^m$	Magnetostrictive coefficient, (ppm/Oe)	3.4(@ 6Oe)

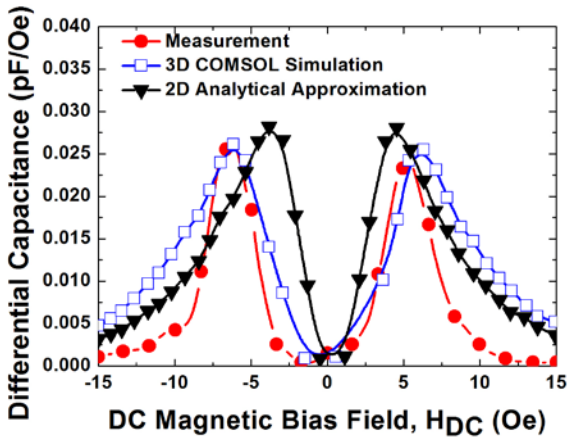

Fig. 9. Differential capacitance versus DC magnetic bias field: comparison between measurement, 3D COMSOL simulation and 2D analytical approximation.

$$d_{eff}(x,y) = 0.5 + \frac{y^2}{18000}\Big|_l + \frac{x^2}{5000}\Big|_w \quad (4)$$

where l is the cantilever length. Taking into accounting both the effective parameters described above, the effective capacitance $C_{eff}(A,d)$ is given by

$$C_{eff} = \frac{\varepsilon_0 A_{eff}}{d_{eff}} = \alpha(A)\varepsilon_0 \int_A \frac{w(1-0.2\frac{2(d-0.5)}{w})}{d}\Delta d$$
$$= \alpha(A)\varepsilon_0 \int_{-w/2}^{w/2}\int_0^l \frac{w(1-0.2\frac{2(\frac{y^2}{18000}+\frac{x^2}{5000})}{w})}{0.5+\frac{2y}{18000}+\frac{2x}{5000}}\Delta x\Delta y \quad (5)$$

and the differential capacitance is given by

$$\Delta C = C_{eff}\frac{\delta}{d_{eff}} \quad (6)$$

where δ is the top flexural gate deflection, which can be calculated as[19, 20]

$$\delta = \frac{3l^2}{t_m}\frac{AB(B+1)}{A^2B^4+2A(2B+3B^2+2B^3)+1}d_{31}^m H_{in} \quad (7)$$

where $A=E_p/E_m$ is Young's modulus ratio, $B=t_p/t_m$ is thickness ratio, $d_{31}{}^m$ is magnetostrictive coefficient, and H_{in} is the input ac magnetic field.

Table 1 summarizes all the parameter values used in the modeling of the for the flexural gate differential capacitance. 3D COMSOL simulations with anticlastic bending (Figure 8(b)) were also performed to compare the results with the experimental and analytical data. The results in Figure 9 show that the model agrees well with the measurements. The overestimation in the modeling result arises due to the aspect ratio difference [7], unaccounted fringing fields of the cantilever etching vias, and the differences between the numerical values of the various parameters and those of the

actual films.

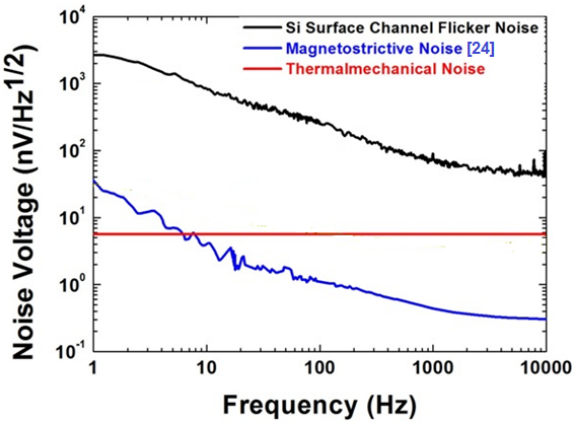

Fig. 11. Noise density of MEFGT. including measured transistor flicker noise, modeled cantilever thermal fluctuation and magnetostrictive noise. The transistor flicker noise is dominant over the entire frequency range.

Figure 10 shows the equivalent circuit of MEFGT. The output signal can now be written as,

$$v_{signal} = \left(g_m \frac{V_{bias}}{C_g + C_p + C_0} r_0 \right) * C_{eff} \frac{\delta}{d_{eff}} \qquad (8)$$

where g_m and r_0 are the transistor transconductance and output resistance respectively, C_g is the input gate capacitance, C_p is the parasitic capacitance, C_0 is the DC air capacitance and V_{bias} is the gate bias voltage. The sensitivity is proportional to the effective air gap capacitance and cantilever deflection.

B. *Noise Modeling*

The overall noise sources in the MEFGT can be divided into three parts: transistor flicker noise, cantilever thermomechanical noise, and magnetostrictive noise. For the transistor in saturation, the expression for flicker noise spectrum is given by [21]

$$S_{vg} = \frac{q^2 N_{ot}}{C_{ox}{}^2 WL} \frac{1}{f} \qquad (9)$$

where C_{ox} is oxide capacitance per unit area, W and L are transistor width and channel length respectively, and N_{ot} is the equivalent oxide trap density. Thermomechanical noise arises as a consequence of the cantilever being in thermal equilibrium with its environment. With the assumption that the thermomechanical noise spectrum is white (i.e. frequency independent), the cantilever deflection noise spectral density can be expressed as [22]

$$S_x = \frac{4k_B T}{k_{eff} \omega_0 Q} \qquad (10)$$

where k_B is the Boltzmann constant, T is the temperature, ω_0 is the resonant frequency, Q is the quality factor, and k_{eff} is effective stiffness constant [23]. By substituting equation (10) into (6) & (8), we can calculate the equivalent cantilever thermomechanical output noise voltage. Magnetostrictive noise also yields a $1/f$ type noise which is indicative of a localized low-frequency relaxation in the magnetostrictive response [24]. Figure 11 summarizes the output noise voltages originating from the three main noise sources. The transistor flicker noise, which is limited by the current fabrication process of surface channel transistors, is the dominant noise source in our MEFGT.

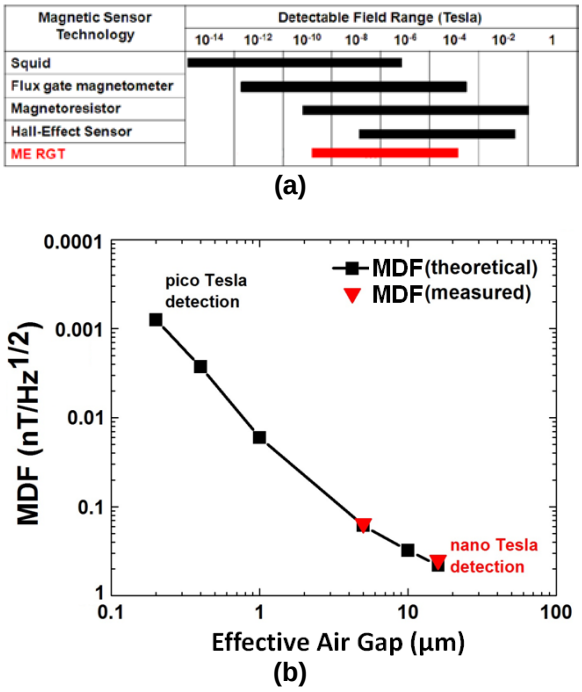

Fig. 12. (a) MEFGT sensitivity benchmarked with current magnetic sensing technologies at 1 Hz. (b) MDF as a function of effective air gap. The MEFGT shows the potential to achieve pico Tesla minimum ac magnetic field detection capability.

VI. Conclusion and Discussion

In summary, we have successfully designed, fabricated, and characterized an integrated Metglas® magnetoelectric flexural transistor capable of nanoTesla detection and picoTesla magnetic fields under resonance condition. In order to achieve this, we have successfully deposited Metglas® films using ion beam sputtering technique. The magnetic properties of the deposited Metglas® films were characterized through the B-H loop and the magnetostrictive properties were measured as

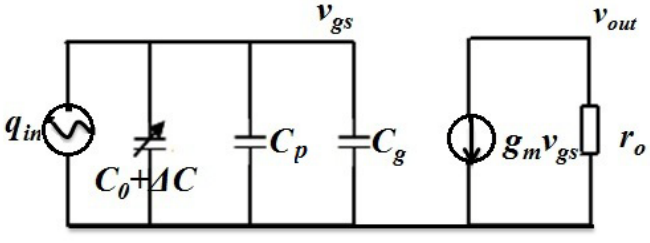

Fig. 10. Small signal equivalent circuit for MEFGT sensor readout system.

function of applied magnetic field. The mechanical resonance of the fabricated cantilever structure was measured to be 4.27

kHz in air and a magnetic field resolution of 60 nT/√Hz (@1 Hz and 150 pT/√Hz at resonance was obtained. The integrated MEMS device using magnetostrictive cantilever and FET sensing and amplification capability exhibits a significant enhancement in the sensitivity and consequently capability better minimum detectable field. This work also demonstrates the direct integration of the ME sensors with Si process technology for implementing ultra sensitive chip-scale magnetometer arrays in highly miniaturized form-factor. The fabricated devices show a clear sensitivity to the direction of the magnetic field with respect to the cantilever length and can thus be used in array format to determine not only the magnitude but also the direction of the magnetic field vector.

By comparing the results in this work to the other current magnetic sensing technology [1-3, 26], we have benchmarked our MEFGT performance in Figure 12 (a). The MEFGT is comparable to the magnetoresistor and has the potential to challenge the flux gate sensors or even SQUID to achieve pico Tesla minimum detectable field. It should be noted that the noise level in our devices is limited by the charge sensing readout transistors. By introducing more advanced buried channel transistors, such as SiGe quantum well FETs [25], there will be a significant reduction in the transistor noise level resulting in an enhanced integrated sensor performance. Furthermore, by achieving a better stress control in the MS cantilever films, it should be possible to fabricated flat cantilever structures with much smaller effective air gap. This will considerably improve the effective sensitivity as shown in Figure 11(b). These considerations suggest the strong potential of the next generation MEFGT in achieving picoTesla detection at 1 Hz in future work.

ACKNOWLEDGMENT

The nanofabrication of the MEFGT was performed at Pennsylvania State University Nanofab supported by the National Nanotechnology Infrastructure Network (NNIN). Also, the authors gratefully acknowledge the support of Jose Israel Ramirez and Thomas Jackson from Pennsylvania State University for the Metglas® Ion Mill sputtering.

REFERENCES

[1] P. Ripka, "Magnetic Sensors and Magnetometers", Ed.. New York: Artech, 2001.
[2] P. Ripka, "Advances in magnetic field sensors", *IEEE Sensors Journal*, Vol. 10, No. 6, 2010.
[3] P. Ripka, "Sensors based on bulk soft magnetic materials: Advances and challenges," *JMMM*, vol. 321, pp. 2466-2473, 2008
[4] R. L. Fagaly, "Spuerconducting quantum interference device instruments and applications," *Rev. Sci. Instruments*, 77, 101101, 2006.
[5] L. D. Landau and E. M.Lifshitz, "Electrodynamics of Continuous Media", pp. 119-120, 1960.
[6] G. T. Rado and V. Folen, "The effective magnetoelectric coefficients of polycrystalline Cr_2O_3 annealed in perpendicular electric and magnetic fields," *J. Phys. Rev. Lett.*, vol. 7, pp. 310, 1961.
[7] Z. Fang, S. G. Lu, F. Li, S. Datta, and Q. M. Zhang, "Enhancing the Magnetoelectric Response of Metglas/Polyvinylidene fluoride Laminates by Exploiting the Flux Concentration Effect," *Appl. Phys. Lett.*, vol. 95, 112903, 2009.
[8] J. Zhai, Z. Xing, S. Dong, J. Li, and D. Viehland, "Detection of pico-Tesla magnetic fields using magnetoelectric sensors at room temperature," *Appl. Phys. Lett.*, vol. 88, 062510, 2006.
[9] F. Li, Z. Fang, R. Misra, S. Tadigadapa, Q. M. Zhang, and S. Datta, "Giant Magnetoelectric Effect in Nanofabricated $Pb(Zr_{0.52}Ti_{0.48})O_3$-$Fe_{0.85}B_{0.05}Si_{0.1}$ Cantilevers and Resonant Gate Transistors," *Device Research Conference*, vol. 37, no. 69, 2011.
[10] H. C. Nathanson. W. E. Newell, R. A. Wickstrom, and Davis J. R. Jr., "The Resonant Gate Transistor," *IEEE Trans. Electron Devices*, vol. 14, no.3, pp.117-133, 1967.
[11] S. Dong, J. Zhai, J. Li, D. Viehland, "Near-ideal magnetoelectricity in high-permeability magnetostrictive piezofibere laminates with a (2-1) connectivity," *Appl. Phys. Lett.*, vol. 89, 252904, 2006.
[12] Y. Wang, D. Gray, D. Berry, J. Gao, M. Li, F. Li, and D. Viehland, "An Extremely Low Equivalent Magnetic Noise Magnetoelectric Sensor," *Adv. Mater.*, vol. 23, pp. 4111–4114, 2011.
[13] F. Li, F. Zhao, Q. M. Zhang and S. Datta, "Low-frequency voltage mode sensing of magnetoelectric sensor in package," *Electronics Letters*, vol. 46, no. 16, 2010.
[14] J. L. Wallace, "Applications of sputtered thin films of magnetoelastic amorphous alloys," *Materials & Design*, vol. 14, no. 5, 1993.
[15] M. Coïsson, C. Appino, F. Celegato, A. Magni, P. Tiberto, and F. Vinai, "Magnetization processes in sputtered FeSiB thin films," *Physical Review B*, vol. 77, 214404, 2008.
[16] F. Li, R. Misra, Z. Fang, C. Curwen, Y. Wu, Q. M. Zhang, P. Schiffer , S. Tadigadapa and S. Datta, "Magnetoelectric Resonant Gate Transistor," accepted by *Solid-State Sensors, Actuators, and Microsystems Workshop*, June 2012.
[17] http://www.comsol.com/ for COMSOL software package.
[18] Y. Lu, and A. Nathan, "Thin film magnetostrictive sensor with on-chip readout and attofarad capacitance resolution," *IEEE Int. Electron Devices Meet.*, pp. 777-780, 1996.
[19] Q. Wang, Q. Zhang, B. Xu, R. Liu, and L. Cross, "Non-linear piezoelectric behavior of ceramic bending mode actuators under strong electric field," *J. Appl. Phys.*, vol. 86, pp. 3352, 1999.
[20] Q. Wang, X. Du, B. Xu, and L. Cross, "Electromechanical coupling and output eciency of piezoelectric bending actuators," *IEEE Trans. on Ultrasonics, Ferro. and Freq. Control*, vol. 46, pp. 638, 1999.
[21] C. Jakobson, I. Bloom, and Y. Nemirovsky, "1/f noise in CMOS transistors for analog applications from subthreshold to saturation," *Solid-State Electron.*, vol. 42, no. 10, pp. 1807–1817, 1998.
[22] K. Y. Yasumura, T. D. Stowe, E. M. Chow, T. Pfafman, T. W. Kenny, B. C. Stipe, and D. Rugar, "Quality Factors in Micron and Submicron Thick Cantilevers," *J. Microelectromech. Syst.*, vol. 9, no. 1, 2000.
[23] S. Pamidighantam, R. Puers, K. Baer tand H. A C Tilmans," Pull-in voltage analysis of electrostatically actuated beam structures with fixed–fixed and fixed–free end conditions," *J. Micromech. Microeng.*, vol. 12, pp. 458–464, 2002.
[24] D. M. Dagenais and F. Bucholtz, "Measurement and origin of magnetostrictive noise limitation in magnetic fiber-optic sensors", *Optics Lett.*, vol. 19, no. 21 , 1994
[25] F. Li, S. H. Lee, Z. Fang, P. Majhi, Q. M. Zhang, S. K. Banerjee, and S. Datta, "Flicker Noise Improvement in 100 nm L_g $Si_{0.50}Ge_{0.50}$ Strained Quantum-Well Transistors using Ultra-Thin Si Cap Layer," *IEEE Electron Device Lett.*, vol. 31, no. 47, 2010.
[26] M. J. Caruso, T. Bratland, C. H. Smith, R. Schneider, *Honeywell, Inc*.

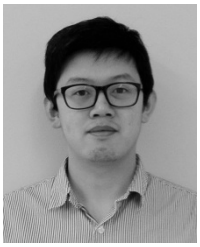

Feng Li received the B.S. degree in Electrical Engineering from Tsinghua University, Beijing, China, in 2008. He is currently working toward the Ph.D. degree in Electrical Engineering in the Department of Electrical Engineering, Pennsylvania State University, University Park.

His research interests include low frequency noise characterization and analysis of Si/SiGe Quantum well FETs as well as design, fabrication, and characterization of chip-scale ultra sensitive magnetometer for biomedical imaging applications.

Rajiv Misra received the B.S. degree in physics and the M.S. degree in computer applications (scientific parallel computing) from the Indian Institute of Technology, Delhi, India, in 1999 and 2002,

respectively, and the Ph.D. degree in physics from University of Florida, Gainesville, in 2009. He is currently postdoctoral Research Associate in the Department of Physics, Pennsylvania State University, University Park.

His research interests include novel magnetic oxides, geometrically frustrated magnets, magnetic nanoparticles, and electronic transport in mesoscopic systems.

Yufei Wu is currently a senior student at Electrical Engineering in the Pennsylvania State University, University Park.

Zhao Fang received B.E. degree in Electronic Engineering from Tsinghua University, Beijing, China, in 2005 and Ph.D. degree in Electrical Engineering from the Pennsylvania State University in 2011. Since then he has been working at Texas Instruments as a Senior Design Engineer.

Peter Schiffer received the B.S. degree from Yale University, New Haven, CT, in 1988 and the Ph.D. degree from Stanford University, Stanford, CA, in 1993.

He is a Professor of Physics and also the Associate Vice President for Research and Director of Strategic Initiatives in the Office of the Vice President for Research at Pennsylvania State University, University Park. Previously, he held a faculty appointment at the University of Notre Dame, Notre Dame, IN, from 1995 to 2000, and was with AT&T Bell Laboratories from 1993 to 1995. He is the author of more than 160 published papers. His research focuses on geometrically frustrated magnets, magnetic semiconductors and oxides, magnetic nanostructures, and granular materials.

Dr. Schiffer is a Fellow of the American Physical Society. He has served as the Chair of the American Physical Society Topical Group on Magnetism and its Applications and as the Program Chair of the 2007 Conference on Magnetism and Magnetic Materials. He will assume the role of Chair of the American Physical Society Division of Materials Physics in 2011. He is the recipient of a Career Award from the National Science Foundation, a Presidential Early Career Award for Scientists and Engineers from the Army Research Office, an Alfred P. Sloan Research Fellowship, and the Faculty Scholar Medal in the Physical Sciences and the Joel and Ruth Spira Award for Teaching Excellence from Penn State.

Qiming Zhang (M'96-SM'00-F'07): Distinguished Professor of Electrical Engineering of Penn State University. Dr. Zhang obtained the Ph.D. degree in 1986 from Penn State University. The research areas in his group include fundamentals and applications of novel electronic and electroactive materials. Research activities in his group cover actuators and sensors, transducers, dielectrics and charge storage devices, polymer thin film devices, polymer MEMS, and electro-optic and photonic devices. He has about 290 publications and 9 patents in these areas. His group has discovered and developed a ferroelectric relaxor polymer which possesses room temperature dielectric constant higher than 50, an electrostrictive strain higher than 7%. His group also proposed and developed nano-polymer composites based on delocalized electron systems to raise the nano-polymeric composites dielectric constant near 1,000. His group demonstrated a new class of polar-polymer with electric energy density over 25 J/cm$_3$, fast discharge speed and low loss, attractive for high efficiency energy storage capacitors. More recently, his group proposed and demonstrated a giant electrocaloric effect at near room temperature in ferroelectric polymers, attractive for on-chip cooling. Many of these results are published in journals of Science and Nature. He is the recipient of the 2008 Penn State Engineering Society Premier Research Award.

Srinivas A. Tadigadapa (SM'12) received the M.S. degree from the Indian Institute of Technology Madras, Chennai, India, and the Ph.D. degree in 1994 from the University of Cambridge, Cambridge, U.K.

From 1996 to 2000, he was the Vice President of Manufacturing of Integrated Sensing Systems Inc. and was involved in the design, fabrication, packaging, reliability, and manufacturing of silicon microsystems. He is currently Professor of electrical engineering and bioengineering at The Pennsylvania State University, University Park. He has been a Research Fellow at the University of Karlsruhe, Karlsruhe, Germany, and Visiting Faculty at Otto von Guericke University, Magdeburg, Germany, and University College, Cork, Ireland. He serves on the Editorial Boards of the *Journal of Microlithography, MEMS and MOEMS* and *Measurement Science and Technology*. His research interests include microsystems, biosensing and exploring phenomenon at the micro–nanointerface.

Dr. Tadigadapa is a fellow of the Institute of Physics, London and a senior member of the IEEE. He received the Alexander von Humboldt Fellowship in Germany and the Walton Fellowship from the Science Foundation of Ireland.

Suman Datta (SM'06) received the B.S. degree in electrical engineering from the Indian Institute of Technology, Kanpur, India, in 1995 and the Ph.D. degree in electrical and computer engineering from the University of Cincinnati, Cincinnati, OH, in 1999.

He is currently Professor of Electrical Engineering, Pennsylvania State University, University Park. From 1999 to 2007, as a member of the Logic Technology Development and Components Research Group at Intel Corporation, he was instrumental in the demonstration of the world's first indium–antimonide based quantum-well transistors operating at room temperature with a record power-delay product, the first experimental demonstration of metal gate plasmon screening and channel strain engineering in high-κ/metal-gate CMOS transistors, and the investigation of the transport properties and the electrostatic robustness in nonplanar "trigate transistors" for extreme scalability. In 2007, he joined Pennsylvania State University as the Joseph Monkowsky Associate Professor for Early Faculty Career Development, exploring new materials, novel nanofabrication techniques, and nonclassical device structures for CMOS "enhancement" as well as "replacement" for future energy-efficient computing applications. He is the author of over 110 archival refereed journal and conference papers. He is the holder of 135 U.S. patents. He is the recipient of the 2012 Penn State Engineering Society Outstanding Research Award.